

Portenga, E.W., Bishop, P., Rood, D.H. and Bierman, P.R. (2017) Combining bulk sediment OSL and meteoric ^{10}Be fingerprinting techniques to identify gully initiation sites and erosion depths. *Journal of Geophysical Research: Earth Surface*, 122(2), pp. 513-527.

There may be differences between this version and the published version. You are advised to consult the publisher's version if you wish to cite from it.

Portenga, E.W., Bishop, P., Rood, D.H. and Bierman, P.R. (2017) Combining bulk sediment OSL and meteoric ^{10}Be fingerprinting techniques to identify gully initiation sites and erosion depths. *Journal of Geophysical Research: Earth Surface*, 122(2), pp. 513-527. (doi:[10.1002/2016JF004052](https://doi.org/10.1002/2016JF004052)) This article may be used for non-commercial purposes in accordance with [Wiley Terms and Conditions for Self-Archiving](#).

<http://eprints.gla.ac.uk/137870/>

Deposited on: 22 May 2017

1 **Combining bulk sediment OSL and meteoric ¹⁰Be fingerprinting techniques to**
2 **identify gully initiation sites and erosion depths**

3
4 **E. W. Portenga^{1,2*}, P. Bishop¹, D. H. Rood^{3,4}, and P. R. Bierman⁵**

5
6 ¹ School of Geographical and Earth Sciences, University of Glasgow, Glasgow, G12 8QQ, UK.

7 ² Department of Environmental Sciences, Macquarie University, North Ryde, NSW 2109,
8 Australia.

9 ³ AMS Laboratory, Scottish Universities Environmental Research Centre, University of
10 Glasgow, East Kilbride G75 0QF, UK.

11 ⁴ Department of Earth Sciences and Engineering, Imperial College London, South Kensington
12 Campus, London SW7 2AZ, UK.

13 ⁵ Geology Department & Rubenstein School of the Environment and Natural Resources,
14 University of Vermont, VT 05405, USA.

15
16 Corresponding author: Eric W. Portenga (ewport@umich.edu)

17 * Now at Department of Earth and Environmental Sciences, University of Michigan, Ann Arbor,
18 MI 48109, USA.

19
20 **Key Points:**

- 21 • First combined use of meteoric ¹⁰Be and bulk OSL to trace sediment back to its source
22 • Sediment source location and depth of initial gully incision are both identified
23 • Gullies eroded initially into livestock-compressed and drought-stressed valley fill, not
24 water-saturated wetlands
25 • Approach can be used to trace sediment in landscapes worldwide, including those
26 disturbed by human activity

29 Abstract

30 Deep erosional gullies dissect landscapes around the world. Existing erosion models focus on
31 predicting where gullies might begin to erode, but identifying where existing gullies were
32 initiated and under what conditions is difficult, especially when historical records are
33 unavailable. Here, we outline a new approach for fingerprinting alluvium and tracing it back to
34 its source by combining bulk sediment optically stimulated luminescence (bulk OSL) and
35 meteoric ^{10}Be ($^{10}\text{Be}_m$) measurements made on gully-derived alluvium samples. In doing so, we
36 identify where gully erosion was initiated and infer the conditions under which such erosion
37 occurred. As both $^{10}\text{Be}_m$ and bulk OSL data have distinctive depth-profiles in different uneroded
38 and depositional settings, we are able to identify the likely depths in potential source areas of
39 alluvium. We demonstrate our technique at Birchams Creek in the southeastern Australian
40 Tablelands – a well-studied and recent example of gully incision that exemplifies a regional
41 landscape transition from unchannelled swampy meadow wetlands to gully incision and
42 subsequent wetland burial by post-European settlement alluvium. We find that such historic
43 alluvium was derived from shallow erosion of valley fill upstream of former swampy meadows
44 and was deposited down the center of the valley. Incision likely followed catchment
45 deforestation and the introduction of livestock, which overgrazed and congregated in valley
46 bottoms in the early 20th century during a period of drought. As a result, severe gully erosion was
47 likely initiated in localized, compacted, and oversteepened reaches of the valley bottom.

48 1.0 Introduction

49 Gullies are deep erosional features incised into landscapes, too large to be easily filled;
50 they can be formed by natural and anthropogenic processes, often involving land-use changes
51 that reduce native vegetation cover [Cox *et al.*, 2010; Eriksson *et al.*, 2006; Eyles, 1977b; Knox,
52 2006; Nyssen *et al.*, 2004; Reusser and Bierman, 2010; Stankoviansky, 2003]. The consequences
53 of gully erosion are two-fold: incision and expansion of gullies in up-catchment landscapes
54 erodes soil [Perroy *et al.*, 2010; Poesen *et al.*, 2003; Reusser and Bierman, 2010], and deposition
55 of gully-derived sediment fills and buries down-catchment landscapes on both short and long
56 term timescales [Beach *et al.*, 2006; Coronato and del Valle, 1993; Eyles, 1977b; Garcia-
57 Rodríguez *et al.*, 2002; Luk *et al.*, 1997; Nichols *et al.*, 2014; Valette-Silver *et al.*, 1986]. While
58 natural gully incision may be unpreventable [Cox *et al.*, 2010; diCenzo and Luk, 1997; Gellis *et al.*,
59 2011; Luk *et al.*, 1997], gully incision following changes in human land-use practices is
60 often, in hindsight, preventable [e.g. Brannstrom and Oliveira, 2000; Eyles, 1977b; Fuchs *et al.*,
61 2004; Montgomery, 2007; Perroy *et al.*, 2010; Reusser and Bierman, 2010; Richardson *et al.*,
62 2014; Rosen, 2008; Stankoviansky, 2003; Turkelboom *et al.*, 2008; Valette-Silver *et al.*, 1986].
63 Whether initiated by natural or anthropogenic causes, gullies affect landscapes around the world,
64 and understanding the conditions under which they are likely to form is crucial to preparing for
65 and possibly mitigating soil and environmental losses resulting from erosion and sediment
66 deposition.

67 Topographic threshold models attempt to predict where gully incision might initiate
68 [Patton and Schumm, 1975; Vandaele *et al.*, 1996]. Other studies show that gully walls and beds
69 become the source of the majority of sediment produced from gullied landscapes [Krause *et al.*,
70 2003; Olley *et al.*, 1993]. However, no studies demonstrate, in the absence of recorded
71 observation, procedures for identifying where in a landscape existing gullies were initiated,

72 information that is necessary to understand the causes of gully erosion. In this study, we outline
73 and test one such procedure.

74 Retrospectively identifying where sediment eroded from gullies originated within a
75 landscape requires a means of monitoring sediment from, or tracing sediment back to, its source.
76 A number of techniques have been used to do this, including radiogenic and cosmogenic
77 isotopes, sediment luminescence, thermochronology, radio tagging, and remote sensing, amongst
78 others [Bradley and Tucker, 2012; D'Haen et al., 2012; Lamarre et al., 2005; Muñoz-Salinas et
79 al., 2014; Nelson et al., 2014; Rengers et al., 2016; Reusser and Bierman, 2010; Stock et al.,
80 2006; Wasson et al., 2002]. When used alone, these techniques can identify detrital sediment
81 source regions, elevations, or lithologies; however, combining multiple techniques has the
82 potential to expand our understanding of geomorphological processes and landforms. For
83 example, multiple geochronometers have been used to independently date landforms such as
84 fault scarps and alluvial surfaces [Bierman et al., 2014; Blisniuk et al., 2012; Nissen et al., 2009]
85 and to understand regolith production and mixing on hillslopes [Dosseto et al., 2008; Ma et al.,
86 2013; West et al., 2013; Wilkinson et al., 2005]. Some techniques have been combined to
87 quantify and monitor sediment transport through fluvial systems, but the number and variety of
88 examples are fewer [e.g. Dosseto and Schaller, 2016; Wasson et al., 2002].

89 Testing ideas about gully incision into landscapes using different sediment tracing
90 techniques requires preservation of sediment deposits that resulted from gully erosion. To this
91 end, the presence of post-(European) settlement alluvium (PSA) in landscapes around the world
92 makes it an ideal such material. Prior to the European colonial era, PSA was often eroded from
93 gully systems that formed as a result of land-use practices being introduced to a landscape that
94 had been previously uninhabited such as in the Americas, Iceland, Africa, Europe, and Asia [e.g.
95 Beach et al., 2006; Coltorti et al., 2010; Dugmore et al., 2000; Kidder et al., 2012; Nyssen et al.,
96 2014; Pope and van Andel, 1984; Rosen, 2008]. More commonly known is landscape erosion
97 and PSA deposition across regions that were affected by European and American colonial
98 expansion and industrial intensification in the 17th–19th centuries throughout North America,
99 South Africa, Europe, Oceania, and South America [e.g. Brannstrom and Oliveira, 2000; Damm
100 and Hagedorn, 2010; Foulds et al., 2013; Garcia-Rodríguez et al., 2002; Montgomery, 2007;
101 Richardson et al., 2014; Portenga et al., 2016a, 2016b; Rustomji and Pietsch, 2007]. Not only is
102 PSA an ideal material for this study because of its connection to gully erosion, but also its
103 relationship to human land use around the world provides insights into the magnitude of
104 historical and pre-historical human impacts on global landscapes and environments [Hooke et al.,
105 2012; Montgomery, 2007; Toy, 1982; Wilkinson and McElroy, 2007].

106 In this study, we combine the sediment fingerprinting capabilities of bulk optically
107 stimulated luminescence (bulk OSL) and meteoric cosmogenic ^{10}Be ($^{10}\text{Be}_m$) to trace PSA
108 deposited in Birchams Creek, a small catchment in the southeastern Australian Tablelands, back
109 to its source. These two techniques have never been applied together in a geomorphological
110 context and we demonstrate how we are able to infer the most reasonable gully erosion history
111 for Birchams Creek by comparing depth profiles of bulk OSL and $^{10}\text{Be}_m$ in PSA and from
112 potential source locations. The widespread use of OSL and $^{10}\text{Be}_m$ in geomorphological studies
113 allows our research approach to be adapted elsewhere to form a more complete understanding of
114 how human land use shapes the landscapes in which people live.

115 2.0 Background

116 2.1 Field Area

117 Widespread gully incision and PSA deposition occurred in the Tablelands region of
118 southeastern Australia (Figure 1), where the causes and timing of gullying and the connection
119 between gullying and PSA deposition have been at the center of research efforts for decades
120 [Crouch, 1987; Eyles, 1977a; Mould and Fryirs, 2017; Muñoz-Salinas et al., 2011, 2014; Neil
121 and Fogarty, 1991; Olley et al., 1993; Olley and Wasson, 2003; Portenga et al., 2016b; Prosser
122 and Slade, 1994; Rustomji and Pietsch, 2007; Starr, 1989; Wasson et al., 1998]. Catchment
123 conditions and land-use practices leading to initial gully incision are often not considered
124 [Prosser and Slade, 1994; Prosser and Winchester, 1996], though they are generally understood
125 to involve vegetation disturbance along valley sides and bottoms, like those imposed by arid
126 climate conditions or those introduced by European settlers in the 19th and 20th centuries [Eyles,
127 1977a, 1977b; Portenga et al., 2016b; Prosser, 1991; Rustomji and Pietsch, 2007; Scott, 2001;
128 Starr, 1989; Zierholz et al., 2001].

129 This study focuses on Birchams Creek, a 3.8 km² headwater tributary of the Yass River
130 about 15 km northeast of Canberra, Australia (Figure 1). Eyles [1977a] studied a chain of ponds
131 in Birchams Creek and its evolution into a continuous gully (Figure 1), a process that occurred
132 regionally soon after European arrival in the early 1800s CE [Eyles, 1977b]. The first surveys of
133 the creek in 1880 CE show swampy meadow wetlands and chains of ponds [Mactaggart et al.,
134 2008] within the lower reaches of the creek before trees were ring barked (e.g. girdled) and
135 cleared in the early 20th century; landowners observed a gully present at the mouth of the creek
136 in 1910 CE [Eyles, 1977a] (Figure 2a). At present, the upper reaches of Birchams Creek are
137 underlain by light-colored loamy distal hillslope deposits, likely with some alluvial component,
138 weathered from the Adaminaby Group, which underlies the whole catchment; we term these
139 sediments valley fill (VF). The lower reaches of the creek had once been characterized by
140 distinctive clayey, organic-rich swampy meadow (SM) wetlands; SM sediments are now overlain
141 by thick deposits of PSA, which were deposited between 1914–1932 CE following European-
142 introduced land-use changes [Portenga et al., 2016a, 2016b].

143 At present, the lower 1.4 km of the Birchams Creek is a deep erosional gully, up to ~4 m
144 deep (Figure 2b-e). Progressing headward from the catchment mouth, stratigraphy exposed in the
145 gully walls are firstly dark clay-rich SM sediment overlain by PSA (site PSA-1; Figure 1), then
146 SM sediment not covered by PSA (site SM-1), another sequence of SM overlain by PSA (site
147 PSA-2), and finally VF (site VF-1), which covers the remainder of the upstream valley bottom
148 (Figure 1). PSA at both sites PSA-1 and PSA-2 is incised by the modern gully – an indication
149 that PSA deposition occurred prior to headward migration of the gully observed in 1910 CE.
150 PSA in Birchams Creek is a sandy loam with lenses of gravel exposed stratigraphically above
151 SM in the lower and middle reaches of Birchams Creek (Figure 1) and can be >1 m thick (Figure
152 3). Though we were unable to map the lateral extent of PSA, it is seen exposed on both sides of
153 gully walls; as elsewhere in the Tablelands, we assume that PSA was deposited across the valley
154 bottoms [Portenga et al., 2016a., 2016b; Rustomji and Pietsch, 2007].

155 Increased overland flow is typically cited as the main triggering mechanism driving gully
156 incision [Poesen et al., 2003; Prosser, 1991; Prosser and Abernethy, 1996], although exactly
157 where within a given drainage overland flow has the greatest effect is uncertain. Field-based
158 flume experiments in the Tablelands have shown that clayey SM sediments resist erosion unless
159 both vegetation is degraded and discharge increased [Prosser and Slade, 1994]; moreover,

160 newly-established swampy vegetation in modern gully beds is able to withstand modern floods
161 [Zierholz *et al.*, 2001]. These findings support the notion that wetlands, though water-saturated,
162 are not likely to be the site of initial gully incision. Others have instead suggested that PSA is
163 more likely derived from erosion into previously-deposited VF sediment [Eyles, 1977a; Prosser,
164 1990; Wasson *et al.*, 1998]. Whether gullies, now regionally common, were more likely to incise
165 into SM sediment or VF is a focus of this study.

166 2.2 Gully initiation conceptual models

167 The majority of sediment transported out of modern gully systems in the Tablelands
168 comes from gully bed and gully bank erosion with minimal sediment being derived from
169 hillslopes [Neil and Fogarty, 1991; Olley *et al.*, 1993]. Assuming, then, that all PSA comes from
170 valley bottom erosion, and not from hillslopes, there are two possible PSA erosional histories at
171 Birchams Creek. In the discontinuous gully erosion conceptual model (DGECEM), gully initiation
172 occurs at multiple locations: alluvium at PSA-1 being sourced from incision at SM-1 at the same
173 time that alluvium at PSA-2 was sourced from incision at VF-1 (Figure 4a). Alternatively, in the
174 single site erosion conceptual model (SSECEM), gully erosion was initiated at VF-1 and supplied
175 alluvium to PSA-1 and PSA-2 (Figure 4b). In the DGECEM, eroded sediment is transported along
176 the modern stream channel, which was later incised by headward erosion of the 1910 CE gully.
177 In the SSECEM, eroded sediment from VF-1 is deposited along the axis of the valley, after which
178 the 1910 CE gully must have eroded from PSA-1 into SM sediments at SM-1 and then back into
179 alluvium at PSA-2.

180 3.0 Methods

181 The uniform bedrock underlying Birchams Creek and its single channel are useful for this
182 study in that measured variations of bulk OSL and $^{10}\text{Be}_m$ concentrations of sediment within the
183 catchment should only result from changes affecting erosion and depositional conditions within
184 the catchment. Luminescence accumulation in mineral grains is directly proportional to the rate
185 and duration of the ‘dose’ of ionizing radiation from the surrounding sediment [Aitken, 1998].
186 Luminescence can be completely removed by sufficient exposure to sunlight during sediment
187 transport – a process called bleaching. However, sediment in fluvial systems is often
188 incompletely bleached [Jain *et al.*, 2004; Rittenour, 2008; Wallinga, 2002], and inherited
189 luminescence has previously been observed for catchments throughout the Tablelands [Muñoz-
190 Salinas *et al.*, 2011, 2014; Olley *et al.*, 1998; Portenga *et al.*, 2016b]. At Birchams Creek, single-
191 grain quartz OSL equivalent doses for PSA at site PSA-1 are bimodal with a clear upper limit,
192 which has been inferred as inheritance from the source material that was incompletely bleached
193 during sediment transport [Portenga *et al.*, 2016b]. Muñoz-Salinas *et al.* [2014] reached a similar
194 conclusion, suggesting that the least completely-bleached fraction of fluvial sediment (i.e. that
195 which is emitted during bulk OSL measurement) is inherited from the sediment’s parent
196 material, which allows that luminescence to be used to trace sediment through a stream network
197 to the sediment’s source. By measuring bulk OSL data in PSA sediment and comparing the
198 results to characteristic bulk OSL profiles of uneroded SM and VF sediments, we are able to
199 infer the geographical source of PSA and the initial incision depth.

200 $^{10}\text{Be}_m$ is produced in the atmosphere through spallogenic interactions between secondary
201 cosmic ray-derived neutrons and O and N target nuclei [Lal and Peters, 1967]. $^{10}\text{Be}_m$ is delivered
202 via precipitation and dry fallout to the Earth’s surface where it is strongly adsorbed to sediment
203 grains and accumulates in soil profiles, forming characteristic depth profiles [Fifield *et al.*, 2010;

204 *Graly et al., 2010; Monaghan et al., 1986; Willenbring and von Blanckenburg, 2010*]. Because
205 $^{10}\text{Be}_m$ adheres strongly to sediment grains, it has been used as a sediment tracer in a number of
206 geomorphic settings [*Brown et al., 1988; Helz and Valette-Silver, 1992; Reusser and Bierman,*
207 *2010*]. Characteristic depth profiles of $^{10}\text{Be}_m$ therefore provide a secondary and independent
208 assessment of PSA sediment provenance and initial incision depth.

209 Sediment samples for both bulk OSL and $^{10}\text{Be}_m$ measurements were collected at each of
210 the four sites in Birchams Creek: PSA-1, PSA-2, SM-1, and VF-1 (Figures 1, 2). Bulk OSL
211 samples were measured at 3 cm depth intervals to a depth of ~1 m at all sites and sediment
212 profile descriptions were recorded (Figure 3); deeper sampling at SM-1 continued at 5 cm
213 intervals. $^{10}\text{Be}_m$ samples were collected as point samples at 9 cm depth intervals at PSA-1, PSA-
214 2, and VF-1, to depths of 102 cm, 75 cm, and 81 cm, respectively, and at 12 cm depth intervals at
215 SM-1 to a depth of 112 cm.

216 Samples were measured for bulk OSL using a portable OSL reader [*Sanderson and*
217 *Murphy, 2010*]. Each polymineral, poly-grain size sample was stimulated by both infrared and
218 blue-light LED sources (60 s, each). Dark counts – photon counts detected in the absence of
219 stimulation – were also measured prior to and after infrared and blue-light stimulation. Photon
220 counts emitted from bulk OSL sediment following stimulation cycles were summed such that
221 each bulk OSL measurement reflects the total luminescence emitted from all grain-sizes and
222 mineral phases in each bulk sediment sample minus the luminescence measured during dark
223 counts (Figure S1). Bulk sediment OSL samples include a large number of grains, making it
224 possible for a few rare, highly-sensitive (e.g. bright) grains to overwhelm the bulk OSL
225 measurement and produce unusually high bulk OSL measurements [*Rhodes, 2007*]. To counter
226 this possible effect, we smoothed the bulk OSL depth-profiles using a 3-sample moving average
227 (Figure 5a). Bulk OSL data from sample replicates measured from well-bleached SM sediments
228 converge on similar values; bulk OSL data from PSA sediment replicates show variability,
229 however, likely resulting from measuring the luminescence of incompletely bleached samples or
230 from the inclusion of a few bright grains (see Figure 4 in [*Portenga et al., 2016a*]). Although
231 PSA exhibits more variable luminescence in replicate sampling, the overall depth trends of bulk
232 OSL data through PSA profiles replicate well, even when measurements are made years apart
233 [*Portenga and Bishop, 2016*].

234 $^{10}\text{Be}_m$ was measured on the same samples as were used for bulk OSL analyses. Soil pH
235 for all samples was measured using powdered pH indicators and values range from 5.5–7; thus,
236 we assume that no $^{10}\text{Be}_m$ has been remobilized after being adsorbed to sediment. $^{10}\text{Be}_m$ samples
237 were processed at the University of Vermont Cosmogenic Nuclide Laboratory where they were
238 milled, and ~0.5 g of powdered sample was mixed with ~0.4 g of ^9Be solution (SPEX 1000
239 ppm). A modification of Stone's [1998] fusion method was used to extract beryllium, which was
240 burned to produce beryllium oxide. Each sample was then mixed with Nb powder at a 1:1 molar
241 ratio before being packed into copper cathodes to be analyzed using accelerator mass
242 spectrometry (AMS) at the Scottish Universities Environmental Research Centre (SUERC) [*Xu*
243 *et al., 2015*]. Measured $^{10}\text{Be}/^9\text{Be}$ ratios were normalized to NIST SRM4325 standard material
244 with a $^{10}\text{Be}/^9\text{Be}$ ratio of 2.79×10^{-11} and blank-corrected using three process blanks (avg. = 1.71
245 $\pm 0.83 \times 10^{-14}$), from which concentrations of $^{10}\text{Be}_m$ are derived; blank corrections were $<0.1\%$
246 of measured $^{10}\text{Be}/^9\text{Be}$ ratios. AMS measurement uncertainties for $^{10}\text{Be}_m$ concentrations are 1σ
247 and average 2% for all samples, and uncertainties in the samples and blanks were propagated in
248 quadrature. $^{10}\text{Be}_m$ sample material from SM-1 at a depth of 63 cm was split and each half of the
249 sample was processed, yielding $^{10}\text{Be}_m$ concentrations of $18.6 \pm 0.44 \times 10^8$ atoms/g and $18.8 \pm$

250 0.34×10^8 atoms/g, a difference of 1.4%. The similarity between these replicate samples
251 demonstrates the reproducibility and consistency of the $^{10}\text{Be}_m$ extraction methods used and the
252 $^{10}\text{Be}_m$ results presented.

253 4.0 Results

254 The SM-PSA transition at PSA-1 and PSA-2 occurs at the depth at which changes in
255 sediment texture and color (Figure 3) and changes in bulk OSL depth trends coincide [*Portenga*
256 *et al.*, 2016a]. Below the SM-PSA transition, bulk OSL measurements in SM sediment at PSA-1
257 and PSA-2 systematically decrease up-profile to the SM-PSA transition at 99 and 72 cm,
258 respectively (Figure 5a). The bulk OSL data at depths below the SM-PSA boundary at PSA-1
259 appear, in the figure, not to increase with depth but this is only because the magnitude of bulk
260 OSL data for these samples is small relative to the bulk OSL maximum values measured in the
261 overlying PSA (Table S1). Luminescence measurements increase above the SM-PSA transition
262 to a maximum 3-sample average value of 3.4×10^6 photon counts at PSA-1 (54 cm) and $2.4 \times$
263 10^6 photon counts at PSA-2 (57 cm). Bulk OSL data from SM-1 are near zero at the valley
264 bottom surface and increase with depth to ~65 cm in the SM exposure (Figure 5a); bulk OSL
265 data at SM-1 exhibit maxima at ~65 cm and ~130 cm. Bulk OSL depth trends at VF-1 show a
266 small bulge in the uppermost 20 cm, beneath which bulk OSL data increase systematically to a
267 depth equal to that of the gully bed (Figure 5a); there is perhaps a third bulk OSL increase at a
268 depth of ~50 cm.

269 $^{10}\text{Be}_m$ measurements are similar throughout PSA profiles and average $8.2 \pm 0.8 \times 10^8$
270 atoms/g and $8.2 \pm 0.3 \times 10^8$ atoms/g at PSA-1 and PSA-2, respectively (Figure 5b, Table S2).
271 The main difference between the profiles is at a depth of 21 cm at PSA-1 where a horizon of
272 coarse gravel is exposed along with fine sandy clay loam (Figure 3a); no such horizon exists at
273 PSA-2. At $16 \pm 0.3 \times 10^8$ atoms/g, the meteoric ^{10}Be content of this horizon at PSA-1
274 corresponds to an isolated increase in $^{10}\text{Be}_m$ well above the average, likely representing the
275 isotopic content of the finer-grained matrix rather than the gravel. Measurements of $^{10}\text{Be}_m$ at SM-
276 1 exhibit an increase in concentration from $8.3 \pm 0.16 \times 10^8$ atoms/g at the surface to $19 \pm 0.39 \times$
277 10^8 atoms/g at 63 cm. Below 63 cm, $^{10}\text{Be}_m$ decreases, but increases once more with depth to $21 \pm$
278 0.39×10^8 atoms/g at 99 cm depth. Concentrations of $^{10}\text{Be}_m$ at VF-1 show a general increase
279 from $4.3 \pm 0.13 \times 10^8$ atoms/g at the surface to $20 \pm 0.35 \times 10^8$ atoms/g at a depth of 63 cm.

280 5.0 Discussion

281 The characteristic depth profiles of measured bulk OSL and $^{10}\text{Be}_m$ data through PSA
282 deposits in Birchams Creek and at potential PSA sources allow us to assess the likelihood of
283 different erosion histories for the creek in a way that would not be possible with one sediment
284 tracing technique alone. While the measured bulk OSL and $^{10}\text{Be}_m$ data we present are specific to
285 Birchams Creek, the combined fingerprinting technique and the interpretation we draw from the
286 two datasets is adaptable elsewhere.

287 5.1 Reliability of bulk OSL and $^{10}\text{Be}_m$ data

288 The depth trends of bulk OSL data through PSA and SM sediments at Birchams Creek
289 resemble SM and SM-PSA profiles found elsewhere in the Tablelands [*Muñoz-Salinas et al.*,
290 2014; *Portenga et al.*, 2016a] (Figure 5a); we note, however, that SM sediments at ~90 cm deep
291 at site SM-1 show a substantial decrease in bulk OSL that is not observed in SM sediment

292 profiles elsewhere in the Tablelands [*Portenga and Bishop, 2016*]. Without further sampling or
293 deriving ages throughout the SM-1 profile, we can only speculate that this decrease may
294 represent a former valley bottom surface. Bulk OSL data previously measured through profiles
295 of weathered bedrock show relatively little luminescence in the uppermost horizons and in
296 increase of bulk OSL data with depth [*Muñoz-Salinas et al., 2014*]. The bulk OSL depth trend at
297 VF-1 is not similar to bulk OSL depth trends through weathered bedrock profiles, but instead
298 appears to consist of up to three sequences of sediment deposited with inherited luminescence,
299 suggested by the increases of bulk OSL in the profile at ~15 cm, ~50 cm, and ~80 cm. Floods
300 deep enough to rise over the gully wall or fast enough to entrain and deposit the gravels present
301 in the uppermost 6 cm at VF-1 are unlikely this far up an already small catchment. Thus, we
302 suggest that the sediment exposed at VF-1 reflects sediment mobilized to the valley bottom by
303 hillslope processes with some degree of inherited luminescence from the sediment's source.

304 Concentrations of $^{10}\text{Be}_m$ in soil depth profiles around the world are typically greatest in
305 the near-surface and decrease with depth [*Graly et al., 2010; Willenbring and von Blanckenburg,*
306 *2010*], though increases of $^{10}\text{Be}_m$ at depth have been observed in saprolite horizons of soil
307 profiles in the nearby Burra Creek catchment [*Fifield et al., 2010*]. Like $^{10}\text{Be}_m$ data from Burra
308 Creek, the $^{10}\text{Be}_m$ increase we observe in the subsurface of the VF-1 profile is at depth; however,
309 we suggest that the increase we observe in Birchams Creek is due to the greater proportion of
310 fine grain sizes at depth at VF-1, which provide a greater surface area onto which $^{10}\text{Be}_m$ is
311 adsorbed (Figure 3).

312 5.2 Identifying PSA source locations and depths

313 PSA deposits throughout the Tablelands were transported and deposited by floods; the
314 higher bulk OSL measurements at the base of PSA compared to that in the uppermost SM
315 sediments indicate that PSA was minimally bleached before deposition and that peak bulk OSL
316 measurements reflect bulk OSL from the PSA source material [*Muñoz-Salinas et al., 2014;*
317 *Portenga and Bishop, 2016; Portenga et al., 2016a*]. Thus, to be considered as a reasonable
318 source for PSA, potential sources of PSA (e.g. SM-1, VF-1) must contain sediment with bulk
319 OSL values greater than or equal to the bulk OSL maxima of PSA deposits (e.g. PSA-1, PSA-2;
320 Figure 5a). Similarly, the initial incision depth of a gully is given by whatever depth is required
321 to erode sediment with bulk OSL data greater than or equal to the bulk OSL maxima of PSA
322 deposits (Figure 5a). Based on the similar and homogeneous inventories of $^{10}\text{Be}_m$ in PSA at
323 PSA-1 and PSA-2 ($\sim 8.2 \times 10^8$ atoms/g), we suggest that potential PSA source locations and
324 depths are determined by averaging the $^{10}\text{Be}_m$ inventories at SM-1 and VF-1 with depth until the
325 average exceeds that of the PSA deposits (Figure 5b).

326 Based on our bulk OSL measurements, the DGECM is only a valid erosion model if SM-
327 1 is incised to a depth between 39–89 cm and VF-1 is incised to a depth of 9–18 cm, thus
328 providing sediment at PSA-1 and PSA-2, respectively, with sufficiently high levels of inherited
329 luminescence (Figure 5, Table 3). VF-1 could be incised to a depth of 81 cm before it exceeds
330 the average $^{10}\text{Be}_m$ concentration at PSA-2, but incising SM-1 to any depth greater than 12 cm
331 results in $^{10}\text{Be}_m$ concentrations significantly greater than that observed at PSA-1. Thus, it follows
332 that because shallow erosion of 9–18 cm at VF-1 adequately explains the $^{10}\text{Be}_m$ and bulk OSL
333 data at PSA-2, it can be considered a source for PSA at PSA-2; however, because there is no
334 overlap at SM-1 of the depths required to supply PSA-1 with both the measured $^{10}\text{Be}_m$ and bulk
335 OSL data, it is not a likely source. Our data therefore do not support the validity of the DGECM
336 in explaining the erosion and PSA deposition history at Birchams Creek. Our data show that bulk

337 OSL measured at PSA-1 could be derived from at least 15 cm of incision at VF-1 and that $^{10}\text{Be}_m$
338 measured at PSA-1 would not be exceeded unless VF-1 was eroded to a depth of >45 cm (Table
339 1); therefore, shallow incision of VF-1 (~15 cm) could also supply adequate amounts of inherited
340 luminescence and $^{10}\text{Be}_m$ to PSA-1 as well as to PSA-2. We therefore conclude that the only
341 plausible erosion scenario for Birchams Creek is the SSECM, in which only VF is incised,
342 releasing sediment that is subsequently deposited downstream as PSA at multiple sites. This
343 conclusion is supported by findings from other studies demonstrating how SM wetlands resist
344 erosion [Prosser and Slade, 1994; Zierholz *et al.*, 2001].

345 We further support our interpretation by showing that shallow incision (15 cm) at and
346 upstream of VF-1 can provide the volume of PSA at PSA-1 and PSA-2 and balance the isotopic
347 budget in the PSA deposits, considering that the valley-bottom ponds from 1880 CE are now also
348 filled with PSA and the whole valley bottom is blanketed by PSA (Figure 1). The volume of the
349 ponds in 1880 CE is 2,510 m³, estimated from maps and pond surface area-depth relationships
350 [Eyles, 1977a]. The remaining volume of PSA deposited across the valley bottom is estimated to
351 be 290 m³, which is the areal extent of areas with low slope ($\leq 1^\circ$, using 30 m-resolution SRTM
352 elevation data [Jarvis *et al.*, 2008]) and a depth of 21 cm at PSA-1 (indicated by the gravel
353 horizon deposited over the filled ponds, Figure 3) and a depth of 63 cm at PSA-2. The total
354 estimated volume of PSA in Birchams Creek is 2,800 m³, and corresponds to a total $^{10}\text{Be}_m$
355 inventory of 3.2×10^{18} atoms, using the average PSA $^{10}\text{Be}_m$ isotopic concentration at PSA-1 and
356 PSA-2. The sediment volume of the PSA deposits is matched by erosion ~15 cm deep and 11.9
357 m wide (average *b*-axis of ponds mapped in 1941 CE) along 3,190 m of the valley bottom at and
358 upstream of VF-1; such erosion along the valley bottom upstream of VF-1 also supplied
359 sufficient $^{10}\text{Be}_m$ to balance the $^{10}\text{Be}_m$ inventory measured from the PSA deposits. Eyles [1977a]
360 shows that 3,730 m of the valley bottom was eroded by 1941 CE meaning that 86% of the
361 sediment derived from initial incision along the eroded length of Birchams Creek is preserved on
362 the landscape as PSA. This result agrees with previous findings showing that the majority of
363 sediment eroded during gully incision in the Tablelands remains close to its source [Melville and
364 Erskine, 1986].

365 5.3 Triggering mechanism for gully erosion at Birchams Creek

366 The timing of PSA deposition at Birchams Creek between 1914–1932 CE is provided
367 both anecdotally and quantitatively [Eyles, 1977a; Portenga *et al.*, 2016b], and this study
368 suggests where and how deep gullies first incised within the watershed. We have yet, however,
369 to identify what triggered erosion in the first place. We explore the likelihood that the shear
370 stress of stream flow associated with increased rainfall during otherwise arid conditions
371 overcame the shear resistance of the valley bottom sediment at VF-1 to trigger gully incision
372 [Melville and Erskine, 1986; Patton and Schumm, 1975; Prosser and Abernethy, 1996; Prosser
373 and Slade, 1994]. The relationship between the critical slope threshold (S_{cr} , given as % gradient)
374 and upstream catchment area (A , in hectares) is provided by $S_{cr} = aA^{-b}$, where a and b are site
375 specific constants that account for local climate and erodibility [Vandaele *et al.*, 1996]. With the
376 exception of Birchams Creek, initial gully incision sites are largely unknown in the Tablelands;
377 thus, S_{cr} and A of gullied creeks are unmeasurable, and a and b cannot be derived empirically.
378 We therefore substitute a range of values, derived for valley-bottom gullies in Europe that have
379 soil textures and mean annual rainfall similar to those at Birchams Creek ($a = 0.025\text{--}0.09$; $b = -$
380 $0.25\text{--}-0.4$) [Vandaele *et al.*, 1996]. The upstream area of Birchams Creek at VF-1 is 306 ha, and
381 the slope of the Birchams Creek valley bottom at VF-1 is $\sim 1^\circ$, which requires $S_{cr} > 1.75$ for

382 incision to occur. Using substituted values of a and b , S_{cr} in Birchams Creek ranges from 0.11–
383 0.89 (or 4.7° – 40°); thus, valley bottom slopes at VF-1, where the gully initially incised, would
384 have to be ~5–40x steeper before incision could occur. Moreover, Eyles [1977a] observed that
385 scour ponds in Birchams Creek are all found on valley bottom surfaces with the shallowest
386 gradients – another indication that no topographic thresholds have been crossed. Thus, Birchams
387 Creek is seemingly not steep enough to erode a gully; yet, erosion still occurred.

388 Vegetated catchments in the Tablelands have the capacity to withstand erosion from
389 severe floods [Neil and Fogarty, 1991; Zierholz et al., 2001]; therefore, if high rainfall triggered
390 gully incision, severe vegetation degradation must have preceded gully initiation. In the early
391 1900s CE, the Tablelands was in the midst of a severe drought, as indicated by the near-total
392 evaporation of endorheic Lake George [Jacobson et al., 1991] (Figure 1). Furthermore, land use
393 changed at this time from open eucalypt woodlands to cleared grazing pastures, which were used
394 both by livestock and feral pigs [Eyles, 1977a]. In addition to overgrazing, the presence of
395 livestock likely compacted soils, thereby decreasing soil infiltration and increasing the stream’s
396 ability to erode [Trimble and Mendel, 1995; Warren et al., 1986]. Elsewhere in the Tablelands,
397 congregating livestock created wallows, or depressions, in cleared valley bottoms that were
398 observed to erode into deep gullies during breaks in severe droughts [Eyles, 1977b]. We
399 therefore argue that livestock wallows in Birchams Creek created highly-localized oversteepened
400 reaches ($\gg S_{cr}$) of the streambed at VF-1, which were then eroded by regionally high rainfall
401 events that broke the drought in the early 1900s CE (see Figure 6 in Portenga et al. [2016b]).
402 Such streamflow could reasonably initiate gully erosion and transport and deposit the PSA now
403 observed in the lower Birchams Creek watershed.

404 The landscape history at Birchams Creek is similar to that documented for nearby
405 Jerrabomberra Creek catchment [Wasson et al., 1998]. Gully incision at both creeks illustrate the
406 effects that European-introduced grazing practices likely had on erosion in the Tablelands, and
407 we therefore suggest that the landscape history of Birchams Creek is representative of erosion
408 histories of small headwater catchments throughout the Tablelands. We recognize, however, that
409 while our explanation for the conditions leading to gully erosion is a plausible and reasonable
410 erosion history for the relatively small Birchams Creek, it is uncertain whether larger catchments
411 behaved similarly. That being said, our techniques and findings suggest that under the right
412 circumstances, combined sediment tracing allows for reconstructions of gully incision, erosion,
413 and sediment deposition to be made, whether brought about by land-use changes or natural
414 thresholds being crossed.

415 **6.0 Conclusions**

416 This study presents a novel dual sediment-fingerprinting technique that combines
417 measurements of bulk OSL and $^{10}\text{Be}_m$ to identify, for the first time, the source location and
418 source depth of gully-derived sediment. We demonstrate this technique in the southeastern
419 Australian Tablelands – one of the most gully-affected landscapes in the world – by tracing PSA
420 sediment deposited in Birchams Creek to its source location and estimating the depth from which
421 it was eroded. In doing so, we test two conceptual models of gully development for the creek,
422 and we confirm that all PSA in the catchment originated from shallow incision into valley fill in
423 the creek’s headwaters that eventually developed into gullies. This finding contrasts with the
424 notion that gully development originated in reaches of the stream that were occupied by water-
425 saturated swampy meadow wetlands. Sediment volumes, measurements of bulk OSL, and
426 isotopic inventories of $^{10}\text{Be}_m$ between upstream erosional sources and downstream depositional

427 locations are balanced, further supporting the notion that erosion of valley fill supplied
 428 downstream reaches of the creek with thick mantles of PSA. Our findings are consistent with
 429 conclusions drawn in nearby studies and with historical documentation. As this study
 430 incorporates a number of assumptions based on available historical documentation and findings
 431 from previous studies, the application of our techniques to assess gully erosion and PSA
 432 deposition in other landscapes around the world may be limited to locations where similar
 433 historical documentation is also available.

434 Acknowledgments and Data

435 This research was funded by a University of Glasgow International PhD Research Studentship
 436 and an International Macquarie University Research Excellence Scholarship. We thank the staff
 437 of the AMS Laboratory at SUERC for their support during beryllium isotopic analyses. The
 438 authors clarify that there are no conflicts of interest, perceived or otherwise, between funding
 439 sources or author affiliations and the outcome of this work. All data are presented in Tables S1
 440 and S2 of the online Supporting Information file. We thank Veronica Sosa-González, Lee
 441 Corbett, Tom Neilson, and Meredith Orr for field and laboratory assistance.

442 Tables

Table 1. Potential PSA source locations and depths

		DGECM		SSECM
		SM-1	VF-1	VF-1
PSA-1	Bulk OSL	39-89 cm 102-147 cm	---	~15 cm 69-99 cm
	¹⁰ Be _m	0-12 cm	---	0-45 cm
PSA-2	Bulk OSL	---	9-18 cm 63-99 cm	9-18 cm 63-99 cm
	¹⁰ Be _m	---	0-81 cm	0-81 cm

443

444 Figure Captions

445 **Figure 1.** The Birchams Creek watershed (BC, shaded white on inset figure) is a tributary of the
 446 Yass River, in the southeastern Australian Tablelands. C – Canberra, Australian Capital
 447 Territory; W – Wamboin, New South Wales. Main figure shows a time series illustrating gully
 448 development in Birchams Creek. The 1880 CE, 1941 CE, and 1975 CE time-steps are adapted
 449 from Eyles (1977a), and the 2013 CE time-step is drawn from satellite imagery and field site
 450 visits. Gully connectivity decreased during 1975–2013 CE as sediment became trapped behind
 451 farm dams (reservoirs) and sealed roads. Lower-case letters indicate locations where photographs
 452 shown in Figure 2 were taken.

453

454 **Figure 2.** Photographs of the field area. Photo locations are shown in Figure 1. (a) The contrast
 455 between totally and partially deforested hillslopes on the low-relief west hillslopes of Birchams
 456 Creek. Lower hillslopes grade into the valley bottom. Photograph taken facing south. (b) Modern
 457 gully with PSA and SM sediments exposed at site PSA-1. Gully walls are ~4 m in height.
 458 Photograph previously used in Portenga et al. [2016a], taken facing upstream. (c) Expansive
 459 modern gully eroding through SM sediments at SM-1. Gully walls are 1–3 m in height. SM-1

460 collected on south exposure. Photograph taken facing west. **(d)** Modern gully wall with PSA and
461 SM sediments exposed at site PSA-2. Gully walls are ~3 m in height. Photograph taken facing
462 downstream. **(e)** Valley fill sediments and distal hillslope deposits incised by the modern gully at
463 VF-1. Sample profile extends to the bottom of the gully bed. Photograph taken facing west. **(f)**
464 Swampy meadow wetlands and pond (in foreground) filling in the modern valley bottom above
465 site VF-1. Ponds have migrated upstream since originally mapped in 1880 CE. Photograph taken
466 facing north.

467
468 **Figure 3.** Photographic and textural descriptions sediment profiles for **(a)** PSA-1, **(b)** PSA-2, **(c)**
469 SM-1, and **(d)** VF-1. Single-grain quartz OSL burial ages of post-European settlement alluvium
470 and swampy meadow sediments at PSA-1 are from Portenga et al. [2016b]. Dashed white lines at
471 PSA-1 and PSA-2 indicate the bulk OSL transition depth from swampy meadow to post-
472 European settlement alluvium sediment accumulation [Portenga et al., 2016a].

473
474 **Figure 4.** Schematic diagrams of profile locations and initial gully erosion models at Birchams
475 Creek. **(a)** The discontinuous gully erosion model (DGECEM) shows alluvium at PSA-1
476 originating in swampy meadow sediments at SM-1 (light blue coloring) and alluvium at PSA-2
477 originating in valley fill sediments at and upstream of VF-1 (dark blue coloring). **(b)** The single
478 site erosion model (SSECEM) shows alluvium at PSA-1 and PSA-2 originating in valley fill
479 sediments at and upstream of VF-1 (orange coloring). Dotted black lines represent areas of
480 erosion while solid black lines represent deposition. Continuous black line is Birchams Creek
481 with black arrows indicating flow direction. Thin colored arrows indicate sediment transport and
482 deposition direction.

483
484 **Figure 5.** Sediment transport pathways inferred from the DGECEM. **(a)** Total bulk sediment OSL
485 (black circles) at each profile site and the 3-sample average bulk OSL used for analyses in this
486 study (black line). Uncertainties are many orders of magnitude less than the data points; thus,
487 uncertainties are not shown, but can be found in Supplementary Table 1. Dashed black lines are
488 at the SM-PSA transition, as interpreted from bulk OSL data and sediment texture descriptions.
489 Solid light and dark blue boxes at PSA-1 and PSA-2, respectively, show the depths of peak
490 inherited OSL. Dashed light and dark blue boxes at SM-1 and VF-1, respectively, indicate the
491 depths where bulk OSL data are greater than or equal to bulk OSL maxima at PSA-1 and PSA-2,
492 and thus represent the potential depths from which PSA at sites PSA-1 and PSA-2, respectively,
493 could have originated under the DGECEM. Bold arrows indicate pathways of sediment
494 transportation from potential sources to PSA deposits. Note x-axis for SM-1 is not the same as
495 the others. **(b)** Concentrations of $^{10}\text{Be}_m$ at each profile site (black circles). Uncertainties are many
496 orders of magnitude less than the data points; thus, uncertainties are not shown, but can be found
497 in Supplementary Table 2. Solid light and dark blue boxes at PSA-1 and PSA-2 indicate the
498 depths over which $^{10}\text{Be}_m$ concentrations are averaged in PSA deposits. Dashed light and dark
499 blue boxes at SM-1 and VF-1 indicate the respective source depths from which PSA at sites
500 PSA-1 and PSA-2 could have originated under the DGECEM. Bold arrows indicate pathways of
501 sediment transport from potential sources to PSA deposits.

502
503 **Figure 6.** Sediment transport pathways inferred from the SSECEM. **(a)** Total bulk sediment OSL
504 (black circles) at each profile site and the 3-sample average bulk OSL used for analyses in this
505 study (black line). Uncertainties are many orders of magnitude less than the data points; thus,

506 uncertainties are not shown, but can be found in Supplementary Table 1. Dashed black lines are
507 at the SM-PSA transition, as interpreted from bulk OSL data and sediment texture descriptions.
508 Solid orange boxes at PSA-1 and PSA-2, respectively, show the depths of peak inherited OSL.
509 Dashed orange box at VF-1 indicates the depths where bulk OSL data are greater than or equal to
510 bulk OSL maxima at PSA-1 and PSA-2, and thus represent the potential depths from which PSA
511 at sites PSA-1 and PSA-2, respectively, could have originated under the SSECM. Bold arrows
512 indicate pathways of sediment transportation from potential sources to PSA deposits. **(b)**
513 Concentrations of $^{10}\text{Be}_m$ at each profile site (black circles). Uncertainties are many orders of
514 magnitude less than the data points; thus, uncertainties are not shown, but can be found in
515 Supplementary Table 2. Solid orange boxes at PSA-1 and PSA-2 indicate the depths over which
516 $^{10}\text{Be}_m$ concentrations are averaged in PSA deposits. Dashed orange box at VF-1 indicates the
517 source depths from which PSA at sites PSA-1 and PSA-2 could have originated under the
518 DGECM. Bold arrows indicate pathways of sediment transport from potential sources to PSA
519 deposits.

520 **References**

- 521 Aitken, M. J. (1998), *An Introduction to Optical Dating: The Dating of Quaternary Sediments by the Use of Photon-*
522 *stimulated Luminescence*, 267 pp., Oxford University Press, Oxford, UK.
- 523 Beach, T., N. Dunning, S. Luzzadder-Beach, D. E. Cook, and J. Lohse (2006) Impacts of the ancient Maya on soils
524 and soil erosion in the central Maya lowlands, *Catena*, 65(2), 166–178, doi:10.1016/j.catena.2005.11.007.
- 525 Bierman, P. R., R. Coppersmith, K. Hanson, J. Neveling, E. W. Portenga, and D. H. Rood (2014) A cosmogenic
526 view of erosion, relief generation, and the age of faulting in southern Africa, *GSA Today*, 24(9), 4–11,
527 doi:10.1130/GSATG206A.1.
- 528 Blisniuk, K., M. Oskin, K. Fletcher, T. Rockwell, and W. Sharp (2012) Assessing the reliability of U-series and ^{10}Be
529 dating techniques on alluvial fans in the Anza Borrego Desert, California, *Quaternary Geochronology*, 13, 26–41,
530 doi: 10.1016/j.quageo.2012.08.004.
- 531 Bradley, N. D., and G. E. Tucker (2012), Measuring gravel transport and dispersion in a mountain river using
532 passive radio tracers, *Earth Surface Processes and Landforms*, 37(10), 1034–1045, doi:10.1002/esp.3223.
- 533 Brannstrom, C. and A. M. S. Oliveira (2000) Human modification of stream valleys in the western plateau of São
534 Paulo, Brazil: implications for environmental narratives and management, *Land Degradation & Development*, 11(6),
535 535–548, doi:10.1002/1099-145X(200011/12)11:6<535::AID-LDR412>3.0.CO;2-L.
- 536 Brown, L., M. J. Pavich, R. E. Hickman, J. Klein, and R. Middleton (1988), Erosion of the eastern United States
537 observed with ^{10}Be , *Earth Surface Processes and Landforms*, 13(5), 441–457, doi:10.1002/esp.3290130509.
- 538 Coltorti, M., J. D. Fazio, F. P. Rios, and G. Tito (2010) The Ñuagapua alluvial fan sequence: Early and Late
539 Holocene human-induced changes in the Bolivian Chaco? *Proceedings of the Geologists' Association*, 121(2), 218–
540 228, doi:10.1016/j.pgeola.2009.11.003.
- 541 Coronato, F. R. and H. F. del Valle (1993) Methodological comparison in the estimate of fluvial erosion in an arid
542 closed basin of northeastern Patagonia, *Journal of Arid Environments*, 24, 231–239, doi:10.1006/jare.1993.1021.
- 543 Cox, R., D. B. Zentner, A. F. M. Rakotondrazafy, and C. F. Rasoazanamparany (2010), Shakedown in Madagascar:
544 Occurrence of lavakas (erosional gullies) associated with seismic activity, *Geology*, 38(2), 179–182,
545 doi:10.1130/G30670.1.
- 546 Crouch, R. J. (1987), The relationship of gully sidewall shape to sediment production, *Australian Journal of Soil*
547 *Research*, 25(4), 531–539.
- 548 Damm, B. and J. Hagedorn (2010) Holocene floodplain formation in the southern Cape region, South Africa,
549 *Geomorphology*, 122, 213–222, doi: 10.1016/j.geomorph.2009.06.025.

550 D'Haen, K., G. Verstraeten, and P. Degryse (2012) Fingerprinting historical fluvial sediment fluxes, *Progress in*
551 *Physical Geography*, 36(2), 154–186, doi:10.1177/0309133311432581.

552 diCenzo, P. D. and S. Luk (1997) Gully erosion and sediment transport in a small subtropical catchment, South
553 China, *Catena*, 29(2), 161–176, doi:10.1016/S0341-8162(96)00053-7.

554 Dosseto, A. and M. Schaller (2016) The erosion response to Quaternary climate change quantified using uranium
555 isotopes and *in situ*-produced cosmogenic nuclides, *Earth-Science Reviews*, 115, 60–81, doi:
556 10.1016/j.earscirev.2016.01.015.

557 Dosseto, A., S. P. Turner, and J. Chappell (2008) The evolution of weathering profiles through time: New insights
558 from uranium-series isotopes, *Earth and Planetary Science Letters*, 274(3–4), 359–371, doi:
559 10.1016/j.epsl.2008.07.050.

560 Dugmore, A. J., A. J. Newton, L. Guðrún, and G. T. Cook (2000) Tephrochronology, environmental change and the
561 Norse settlement of Iceland, *Environmental Archaeology*, 5(1), 21–34, doi:10.1179/env.2000.5.1.21.

562 Eriksson, M. G., J. M. Olley, D. R. Kilham, T. Pietsch, and R. J. Wasson (2006), Aggradation and incision since the
563 very late Pleistocene in the Naas River, south-eastern Australia, *Geomorphology*, 81(1–2), 66–88,
564 doi:10.1016/j.geomorph.2006.04.001.

565 Eyles, R. J. (1977a), Birchams Creek: the transition from a chain of ponds to a gully, *Australian Geographical*
566 *Studies*, 15(2), 146–157, doi:10.1111/j.1467-8470.1977.tb00094.x.

567 Eyles, R. J. (1977b), Changes in drainage networks since 1820, Southern Tablelands, N.S.W, *Australian*
568 *Geographer*, 13(6), 377–386, doi:10.1080/00049187708702716.

569 Fifield, L. K., R. J. Wasson, B. Pillans, and J. O. H. Stone (2010), The longevity of hillslope soil in SE and NW
570 Australia, *Catena*, 81(1), 32–42, doi:10.1016/j.catena.2010.01.003.

571 Foulds, S. A., M. G. Macklin, and P. A. Brewer (2013) Agro-industrial alluvium in the Swale catchment, northern
572 England, as an event marker for the Anthropocene, *The Holocene*, 0(0), 1–16, doi: 10.1177/0959683612465445.

573 Fuchs, M., A. Lang, and G. A. Wagner (2004) The history of Holocene soil erosion in the Phlious Basin, NE
574 Peloponnese, Greece, based on optical dating, *The Holocene*, 14(3), 334–345, doi: 10.1191/0959683604hl710rp.

575 Gellis, A. C., M. J. Pavich, A. L. Ellwein, S. Aby, I. Clark, M. E. Wiczorek, and R. Viger (2011) Erosion, storage,
576 and transport of sediment in two subbasins of the Rio Puerco, New Mexico, *Geological Society of America Bulletin*,
577 124(5–6), 817–841, doi: 10.1130/B30392.1.

578 Graly, J. A., P. R. Bierman, L. J. Reusser, and M. J. Pavich (2010), Meteoric ¹⁰Be in soil profiles - A global meta-
579 analysis, *Geochimica et Cosmochimica Acta*, 74(23), 6814–6829, doi:10.1016/j.gca.2010.08.036.

580 Helz, G. R., and N. Valette-Silver (1992), Beryllium-10 in Chesapeake Bay sediments: an indicator of sediment
581 provenance, *Estuarine, Coastal and Shelf Science*, 34(5), 459–469, doi:10.1016/S0272-7714(05)80117-9.

582 Hooke, R. L., J. F. Martín-Duque, and J. Pedraza (2012) Land transformation by humans: a review, *GSA Today*,
583 22(12), 4–10, doi:10.1130/GSAT151A.1.

584 Jacobson, G., J. Jankowski, and R. S. Abell (1991), Groundwater and surface water interaction at Lake George, New
585 South Wales, *BMR Journal of Australian Geology and Geophysics*, 12, 161–190.

586 Jain, M., A. S. Murray, and L. Bøtter-Jensen (2004) Optically stimulated luminescence dating: How significant is
587 incomplete light exposure in fluvial environments? *Quaternaire*, 15, 143–157, doi:10.3406/quate.2004.1762.

588 Jarvis, A., H. I. Reuter, A. Nelson, and E. Guevara (2008) Hole-filled seamless SRTM data V5, International Centre
589 for Tropical Agriculture (CIAT), available from <http://srtm.csi.cgiar.org>.

590 Kidder, T., L. Haiwang, Q. Xu, and M. Li (2012) The alluvial geoarchaeology of the Sanyangzhuang Site on the
591 Yellow River floodplain, Hanan Province, China, *Geoarchaeology*, 27(4), 324–343, doi:10.1002/gea.21411.

592 Knox, J. C. (2006), Floodplain sedimentation in the Upper Mississippi Valley: Natural versus human accelerated,
593 *Geomorphology*, 79, 286–310, doi:10.1016/j.geomorph.2006.06.031.

- 594 Krause, A. K., S. W. Franks, J. D. Kalma, R. J. Loughran, and J. S. Rowan (2003), Multi-parameter fingerprinting of
595 sediment deposition in a small gullied catchment in SE Australia, *Catena*, 53, 327–348, doi: 10.1016/S0341-
596 8162(03)00085-7.
- 597 Lal, D., and B. Peters (1967), Cosmic ray produced radioactivity on the earth, in *Handbuch der Physik*, edited by K.
598 Sitte, pp. 551–612, Springer-Verlag, New York.
- 599 Lamarre, H., B. MacVicar, and A. G. Roy (2005), Using Passive Integrated Transponder (PIT) Tags to Investigate
600 Sediment Transport in Gravel-Bed Rivers, *Journal of Sedimentary Research*, 75(4), 736–741,
601 doi:10.2110/jsr.2005.059
- 602 Luk, S. H., Q. Y. Yao, J. Q. Gao, J. Q. Zhang, Y. G. He, and S. M. Huang (1997) Environmental analysis of soil
603 erosion in Guangdong Province: A Deqing case study, *Catena*, 29(2), 97–113, doi:10.1016/S0341-8162(96)00049-
604 5.
- 605 Ma, L., F. Chabaux, N. West, E. Kirby, L. Jin, and S. Brantley (2013) Regolith production and transport in the
606 Susquehanna Shale Hills Critical Zone Observatory, Part 1: Insights from U-series isotopes, *Journal of Geophysical*
607 *Research: Earth Surface*, 118(2), 722–740, doi: 10.1002/jgrf.20037.
- 608 Mactaggart, B., J. Bauer, D. Goldney, and A. Rawson (2008), Problems in naming and defining the swampy
609 meadow - An Australian perspective, *Journal of Environmental Management*, 87(3), 461–473,
610 doi:10.1016/j.jenvman.2007.01.030.
- 611 Melville, M. D., and W. Erskine (1986), Sediment remobilization and storage by discontinuous gullying in humid
612 southeastern Australia, in *Drainage Basin Sediment Delivery*, edited by R. F. Hadley, pp. 277–286, International
613 Association of Hydrological Sciences.
- 614 Monaghan, M. C., S. Krishnaswami, and K. K. Turekian (1986), The global-average production rate of ^{10}Be , *Earth*
615 *and Planetary Science Letters*, 76(3–4), 279–287, doi:10.1016/0012-821X(86)90079-8.
- 616 Montgomery, D. R. (2007) *Dirt: The Erosion of Civilizations*, Berkeley, California, USA, University of California
617 Press, 295 p.
- 618 Mould, S and K. Fryirs, 2017, The Holocene evolution and geomorphology of a chain of ponds, southeast Australia:
619 Establishing a physical template for river management, *Catena*, 149, 349–362, doi:10.1016/j.catena.2016.10.012.
- 620 Muñoz-Salinas, E., P. Bishop, D. C. W. Sanderson, and J.-J. Zamorano (2011) Interpreting luminescence data from
621 a portable OSL reader: three case studies in fluvial settings, *Earth Surface Processes and Landforms*, 36(5), 651–
622 660, doi:10.1002/esp.2084.
- 623 Muñoz-Salinas, E., P. Bishop, D. Sanderson, and T. Kinnaird (2014), Using OSL to assess hypotheses related to the
624 impacts of land-use change with the early nineteenth century arrival of Europeans in south-eastern Australia: An
625 exploratory case study from Grabben Gullen Creek, New South Wales, *Earth Surface Processes and Landforms*,
626 39(12), 1576–1586, doi:10.1002/esp.3542.
- 627 Neil, D., and P. Fogarty (1991), Land use and sediment yield on the southern Tablelands of New South Wales,
628 *Australian Journal of Soil and Water Conservation*, 4(2), 33–39.
- 629 Nelson, A. H., P. R. Bierman, J. D. Shakun, and D. H. Rood (2014), Using *in situ* cosmogenic ^{10}Be to identify the
630 source of sediment leaving Greenland, *Earth Surface Processes and Landforms*, 39, 1087–1100,
631 doi:10.1002/esp.3565.
- 632 Nichols, K. K., P. R. Bierman, and D. H. Rood (2014), ^{10}Be constrains the sediment sources and sediment yield to
633 the Great Barrier Reef from the tropical Barron River catchment, Queensland, Australia, *Geomorphology*, 224, 102–
634 110, doi:10.1016/j.geomorph.2014.07.019.
- 635 Nissen, E. R. T. Walker, A. Bayasgalan, A. Carter, M. Fattahi, E. Molor, C. Schnabel, A. J. West, and S. Xu (2009)
636 The late Quaternary slip-rate of the Har-Us-Nuur fault (Mongolian Altai) from cosmogenic ^{10}Be and luminescence
637 dating, *Earth and Planetary Science Letters*, 286(3–4), 467–478, doi:10.1016/j.epsl.2009.06.048.
- 638 Nyssen, J., J. Poesen, J. Moeyersons, J. Deckers, M. Haile, and A. Lang (2004), Human impact on the environment
639 in the Ethiopian and Eritrean highlands - a state of the art, *Earth-Science Reviews*, 64, 273–320.

640 Olley, J., G. Caitcheon, and A. Murray (1998), The distribution of apparent dose as determined by Optically
641 Stimulated Luminescence in small aliquots of fluvial quartz: Implications for dating young sediments, *Quaternary*
642 *Geochronology*, 17(11), 1033–1040, doi:10.1016/S0277-3791(97)00090-5.

643 Olley, J. M., A. S. Murray, D. H. Mackenzie, and K. Edwards (1993), Identifying sediment sources in a gullied
644 catchment using natural and anthropogenic radioactivity, *Water Resources Research*, 29(4), 1037–1043,
645 doi:10.1029/92wr02710.

646 Olley, J. M., and R. J. Wasson (2003), Changes in the flux of sediment in the Upper Murrumbidgee catchment,
647 Southeastern Australia, since European settlement, *Hydrological Processes*, 17(16), 3307–3320,
648 doi:10.1002/hyp.1388.

649 Patton, P. C., and S. A. Schumm (1975), Gully erosion, northwestern Colorado: A threshold phenomenon, *Geology*,
650 3(2), 88–90, doi:10.1130/0091-7613(1975)3<88:GENCAT>2.0.CO;2.

651 Perroy, R. L., B. Bookhagen, G. P. Asner, and O. A. Chadwick (2010) Comparison of gully erosion estimates using
652 airborne and ground-based LiDAR on Santa Cruz Island, California, *Geomorphology*, 118(3–4), 288–300,
653 doi:10.1016/j.geomorph.2010.01.009.

654 Poesen, J., J. Nachtergaele, G. Verstraeten, and C. Valentin (2003), Gully erosion and environmental change:
655 importance and research needs, *Catena*, 50, 91–133, doi:10.1016/S0341-8162(02)00143-1.

656 Pope, K. O. and T. H. van Andel (1984) Late Quaternary alluviation and soil formation in the southern ARgoldid: Its
657 history, causes and archaeological implications, *Journal of Archaeological Science*, 11(4), 281–306,
658 doi:10.1016/0305-4403(84)90012-8.

659 Portenga, E. W., and P. Bishop (2016), Confirming geomorphological interpretations based on portable OSL reader
660 data, *Earth Surface Processes and Landforms*, 41(3), 427–432, doi:10.1002/esp.3834.

661 Portenga, E. W., P. Bishop, D. B. Gore, and K. E. Westaway (2016a), Landscape preservation under post-European
662 settlement alluvium in the south-eastern Australian tablelands, inferred from portable OSL reader data, *Earth*
663 *Surface Processes and Landforms*, doi:10.1002/esp.3942.

664 Portenga, E. W., K. E. Westaway, and P. Bishop (2016b), Timing of post-European settlement alluvium deposition
665 in SE Australia: A legacy of European land-use in the Goulburn Plains, *The Holocene*,
666 doi:10.1177/0959683616640047

667 Prosser, I. P. (1990), Fire, humans, and denudation at Wangrah Creek, southern Tablelands, N.S.W., *Australian*
668 *Geographical Studies*, 28(1), 77–95, doi:10.1111/j.1467-8470.1990.tb00623.x.

669 Prosser, I. P. (1991), A comparison of past and present episodes of gully erosion at Wangrah Creek, southern
670 Tablelands, New South Wales, *Australian Geographical Studies*, 29(1), 139–154, doi:10.1111/j.1467-
671 8470.1991.tb00711.x.

672 Prosser, I. P., and B. Abernethy (1996), Predicting the topographic limits to a gully network using a digital terrain
673 model and process thresholds, *Water Resources Research*, 32(7), 2289–2298.

674 Prosser, I. P., and C. J. Slade (1994), Gully formation and the role of valley-floor vegetation, southeastern Australia,
675 *Geology*, 22(12), 1127–1130, doi:10.1130/0091-7613(1994)022<1127:gfatro>2.3.co;2.

676 Prosser, I. P., and S. J. Winchester (1996), History and processes of gully initiation and development in eastern
677 Australia, *Zeitschrift für Geomorphologie, Supplementband 105*, 91–109.

678 Rengers, F. K., G. E. Tucker, J. A. Moody, and B. A. Ebel (2016), Illuminating wildfire erosion and deposition
679 patterns with repeat terrestrial lidar, *Journal of Geophysical Research: Earth Surface*, 121(3), 588–608,
680 doi:10.1002/2015JF003600.

681 Reusser, L. J., and P. R. Bierman (2010), Using meteoric ¹⁰Be to track fluvial sand through the Waipaoa River basin,
682 New Zealand, *Geology*, 38(1), 47–50, doi:10.1130/g30395.1.

683 Rhodes, E. J. (2007) Quartz single grain OSL sensitivity distributions: implications for multiple grain single aliquot
684 dating, *Geochronometria*, 26, 19–29, doi:10.2478/v10003-007-0002-5.

685 Richardson, J. M., I. C. Fuller, K. A. Holt, N. J. Litchfield, and M. G. Macklin (2014) Rapid post-settlement
686 floodplain accumulation in Northland, New Zealand, *Catena*, 113, 292–305, doi:10.1016/j.catena.2013.08.013.

687 Rittenour, T. M. (2008) Luminescence dating of fluvial deposits; applications to geomorphic, palaeoseismic and
688 archaeological research, *Boreas*, 37, 613–635, doi:10.1111/j.1502-3885.2008.00056.x.

689 Rosen, A. M. (2008) The impact of environmental change and human land use on the alluvial valleys in the Loess
690 Plateau of China during the Middle Holocene, *Geomorphology*, 101(1–2), 298–307,
691 doi:10.1016/j.geomorph.2008.05.017.

692 Rustomji, P., and T. Pietsch (2007), Alluvial sedimentation rates from southeastern Australia indicate post-European
693 settlement landscape recovery, *Geomorphology*, 90(1–2), 73–90, doi:10.1016/j.geomorph.2007.01.009.

694 Sanderson, D. C. W., and S. Murphy (2010), Using simple portable OSL measurements and laboratory
695 characterisation to help understand complex and heterogeneous sediment sequences for luminescence dating,
696 *Quaternary Geochronology*, 5(2-3), 299–305, doi:10.1016/j.quageo.2009.02.001.

697 Scott, A. (2001), Water erosion in the Murray-Darling Basin: Learning from the past, *Technical Report Rep. 43/01*,
698 134 pp, CSIRO Land & Water.

699 Stankoviansky, M. (2003), Historical evolution of permanent gullies in the Myjava Hill Land, Slovakia, *Catena*, 51,
700 223–239, doi:10.1016/S0341-8162(02)00167-4.

701 Starr, B. (1989), Anecdotal and relic evidence of the history of gully erosion and sediment movement in the
702 Michelago Creek catchment area, NSW, *Australian Journal of Soil and Water Conservation*, 2(3), 26–31.

703 Stock, G. M., T. A. Ehlers, and K. A. Farley (2006), Where does sediment come from? Quantifying catchment
704 erosion with detrital apatite (U-Th)/He thermochronometry, *Geology*, 34(9), 725–728, doi:10.1130/G22592.1.

705 Stone, J. (1998), A rapid fusion method for separation of beryllium-10 from soils and silicates, *Geochimica et*
706 *Cosmochimica Acta*, 62(3), 555–561.

707 Toy, T. J. (1982) Accelerated erosion: process, problems, and prognosis, *Geology*, 10, 524–529, doi: 10.1130/0091-
708 7613(1982)10<524:AEPPAP>2.0.CO;2.

709 Trimble, S. W., and A. C. Mendel (1995), The cow as a geomorphic agent – A critical review, *Geomorphology*, 13,
710 233–253.

711 Turkelboom, F., J. Poesen, and G. Trébuil (2008) The multiple land degradation effects caused by land-use
712 intensification in tropical steepplands: A catchment study from northern Thailand, *Catena*, 75, 102–116,
713 doi:10.1016/j.catena.2008.04.012.

714 Valette-Silver, J. N., L. Brown, M. Pavich, J. Klein, and R. Middleton (1986) Detection of erosion events using ¹⁰Be
715 profiles: example of the impact of agriculture on soil erosion in the Chesapeake Bay area (U.S.A.), *Earth and*
716 *Planetary Science Letters*, 80(1–2), 82–90, doi:10.1016/0012-821X(86)90021-X.

717 Vandaele, K., J. Poesen, G. Govers, and B. van Wesemael (1996), Geomorphic threshold conditions for ephemeral
718 gully incision, *Geomorphology*, 16, 161–173, doi:10.1016/0169-555X(95)00141-Q.

719 Wallinga, J. (2002) Optically stimulated luminescence dating of fluvial deposits: a review, *Boreas*, 31, 303–322,
720 doi:10.1111/j.1502-3885.2002.tb01076.x.

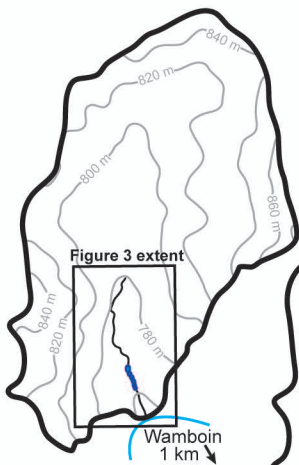
721 Warren, S. D., T. L. Thurow, W. H. Blackburn, and N. E. Garza (1986), The influence of livestock trampling under
722 intensive rotation grazing on soil hydrologic characteristics, *Journal of Range Management*, 39(6), 491–495.

723 Wasson, R. J., G. Caitcheon, A. S. Murray, M. McCulloch, and J. Quade (2002) Sourcing sediment using multiple
724 tracers in the catchment of Lake Argyle, northwestern Australia, *Environmental Management*, 29(5), 634–646,
725 doi:10.1007/s00267-001-0049-4.

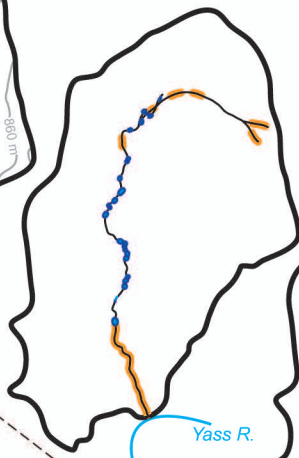
726 Wasson, R. J., R. K. Mazari, B. Starr, and G. Clifton (1998), The recent history of erosion and sedimentation on the
727 Southern Tablelands of southeastern Australia: sediment flux dominated by channel incision, *Geomorphology*,
728 24(4), 291–308, doi:10.1016/S0169-555X(98)00019-1.

- 729 West, N., E. Kirby, P. Bierman, R. Slingerland, L. Ma, D. Rood, and S. Brantley (2013) Regolith production and
730 transport in the Susquehanna Shale Hills Critical Zone Observatory, Part 2: Insights from meteoric ^{10}Be , *Journal of*
731 *Geophysical Research: Earth Surface*, 118(3), 1877–1890, doi: 10.1002/jgrf.20121.
- 732 Wilkinson, M. T., and G. S. Humphreys (2005), Exploring pedogenesis via nuclide-based soil production rates and
733 OSL-based bioturbation rates, *Australian Journal of Soil Research*, 43(6), 767–779, doi:10.1071/SR04158.
- 734 Wilkinson, B. H. and B. J. McElroy (2007) The impact of humans on continental erosion and sedimentation,
735 *Geological Society of America Bulletin*, 119(1–2), 140–156, doi:10.1130/B25899.1.
- 736 Willenbring, J. K., and F. von Blanckenburg (2010), Meteoric cosmogenic Beryllium-10 adsorbed to river sediment
737 and soil: Applications for Earth-surface dynamics, *Earth-Science Reviews*, 98(1–2), 105–122.
- 738 Xu, S., S. P. H. T. Freeman, D. H. Rood, and R. M. Shanks (2015) Decadal ^{10}Be , ^{26}Al and ^{36}Cl QA measurements on
739 the SUERC accelerator mass spectrometer, *Nuclear Instruments and Methods B: Beam Interactions with Materials*
740 *and Atoms*, 361, 39–42, doi:10.1016/j.nimb.2015.03.064.
- 741 Zierholz, C., I. P. Prosser, P. J. Fogarty, and P. Rustomji (2001), In-stream wetlands and their significance for
742 channel filling and the catchment sediment budget, Jugiong Creek, New South Wales, *Geomorphology*, 38(3–4),
743 221–235.

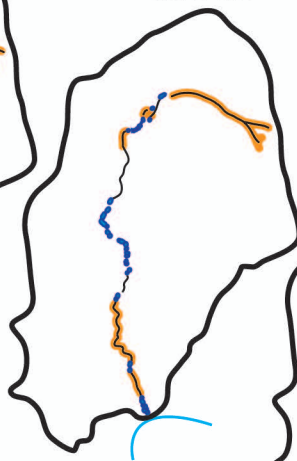
1880 CE



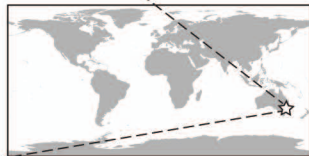
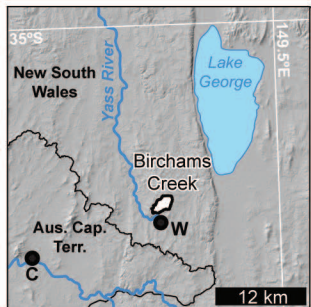
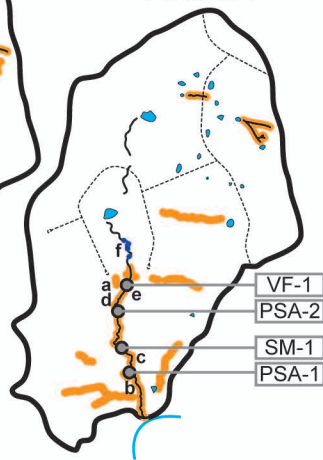
1941 CE



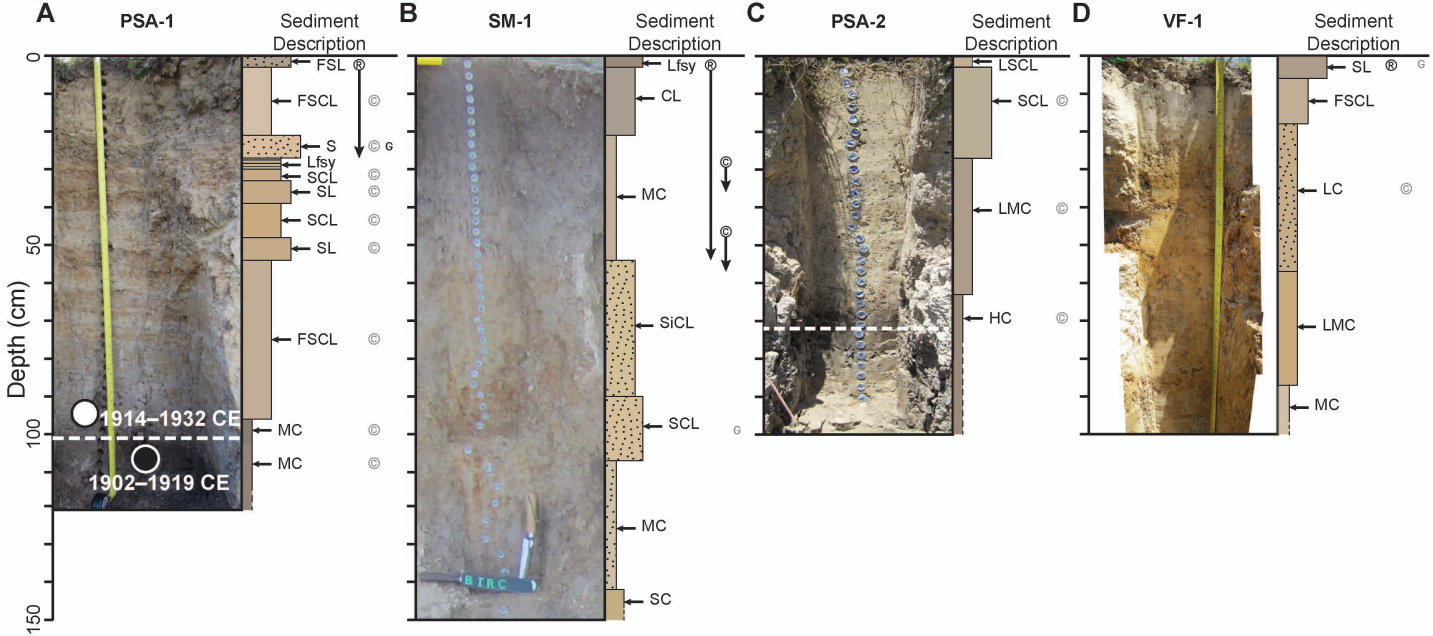
1975 CE



2013 CE

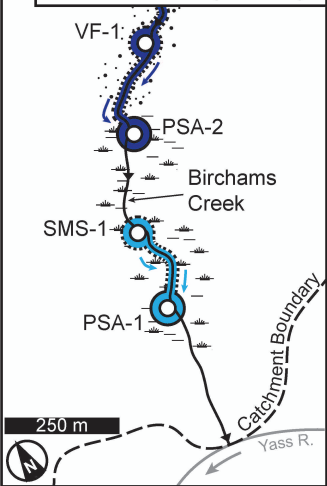




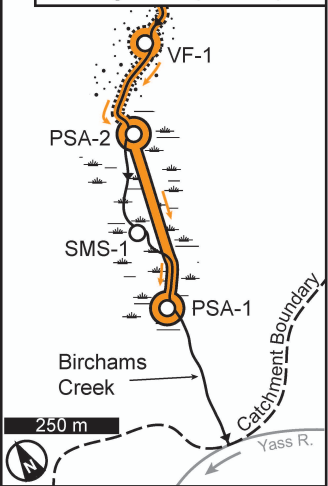


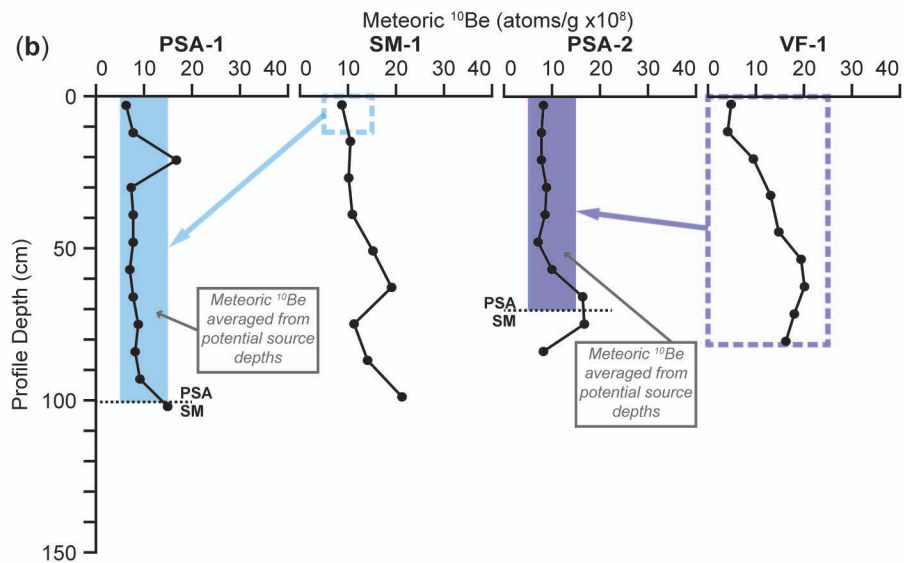
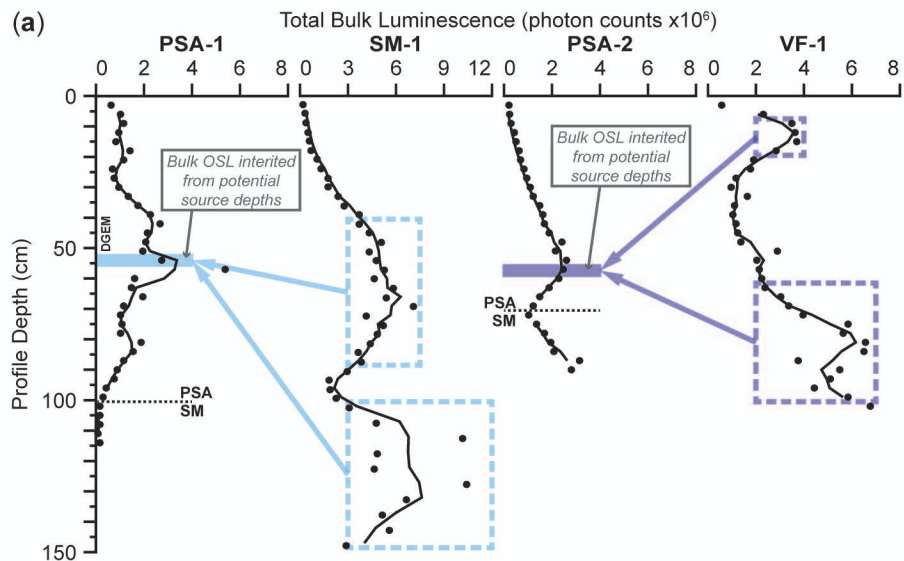
S - Sand	FSCL - Fine sandy clay loam	G	Gravel present at specific depth	Ⓡ	Roots present
SL - Sandy loam	SiCL - Silty clay loam	G	Gravel present in unit	↓	Root depth extent
FSL - Fine sandy loam	SC - Sandy clay	Ⓢ	Charcoal present		Textures colored by Munsell colour
LSCl - Light sandy clay loam	LC - Light clay	↓	Charcoal depth extent		□ No internal structure
Lfsy - Loam, fine sandy	LMC - Light medium clay	Ⓢ	Charcoal present in unit		▨ Laminated structure
SCL - Sandy clay loam	MC - Medium clay	●	PSA quartz OSL burial age		▩ Sandy structure
SiCL - Silty clay loam	HC - Heavy clay		SM quartz OSL burial age		

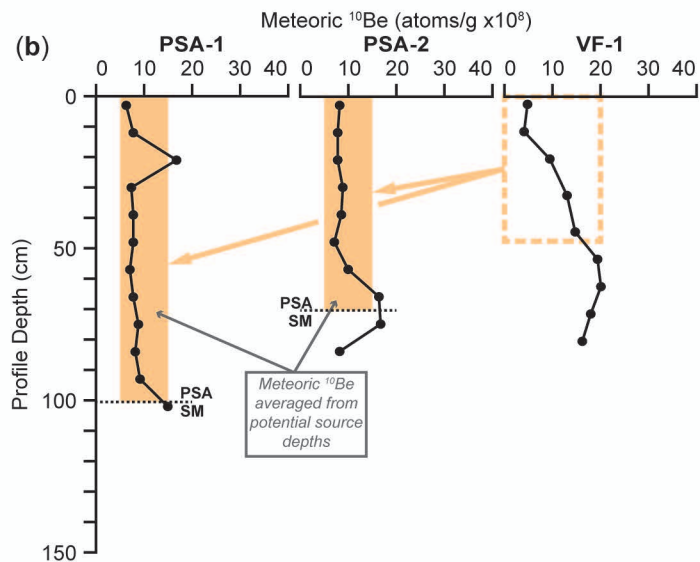
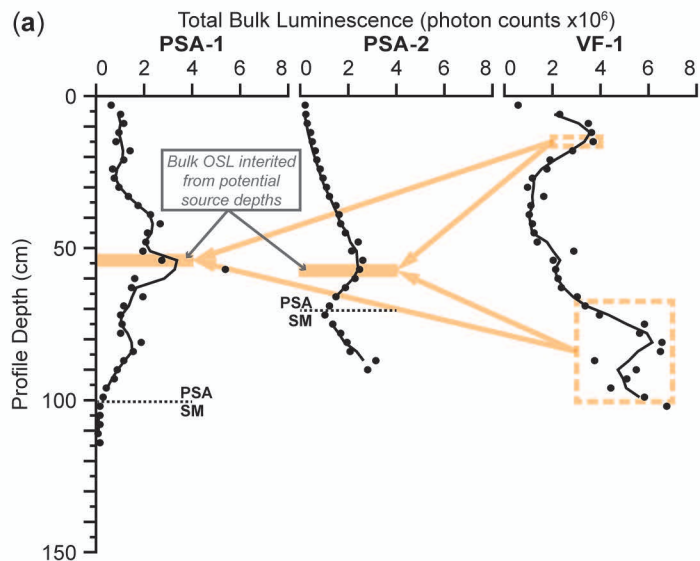
A Discontinuous (DGECM)



B Single Site (SSECM)







Supporting Information for

Combining bulk OSL and meteoric ^{10}Be fingerprinting techniques to identify gully initiation sites and erosion depths

E. W. Portenga^{1,2*}, P. Bishop¹, D. H. Rood^{3,4}, and P. R. Bierman⁵

¹ School of Geographical and Earth Sciences, University of Glasgow, Glasgow, G12 8QQ, UK.

² Department of Environmental Sciences, Macquarie University, North Ryde, NSW 2109, Australia.

³ AMS Laboratory, Scottish Universities Environmental Research Centre, University of Glasgow, East Kilbride G75 0QF, UK.

⁴ Department of Earth Sciences and Engineering, Imperial College London, South Kensington Campus, London SW7 2AZ, UK.

⁵ Geology Department & Rubenstein School of the Environment and Natural Resources, University of Vermont, VT 05405, USA

* Now at Department of Earth and Environmental Sciences, University of Michigan, Ann Arbor, MI 48109, USA.

Contents of this file

Supplementary Figure 1 – Graphical description of bulk OSL measurements

Supplementary Table 1 – Bulk OSL data

Supplementary Table 2 – Meteoric ^{10}Be data

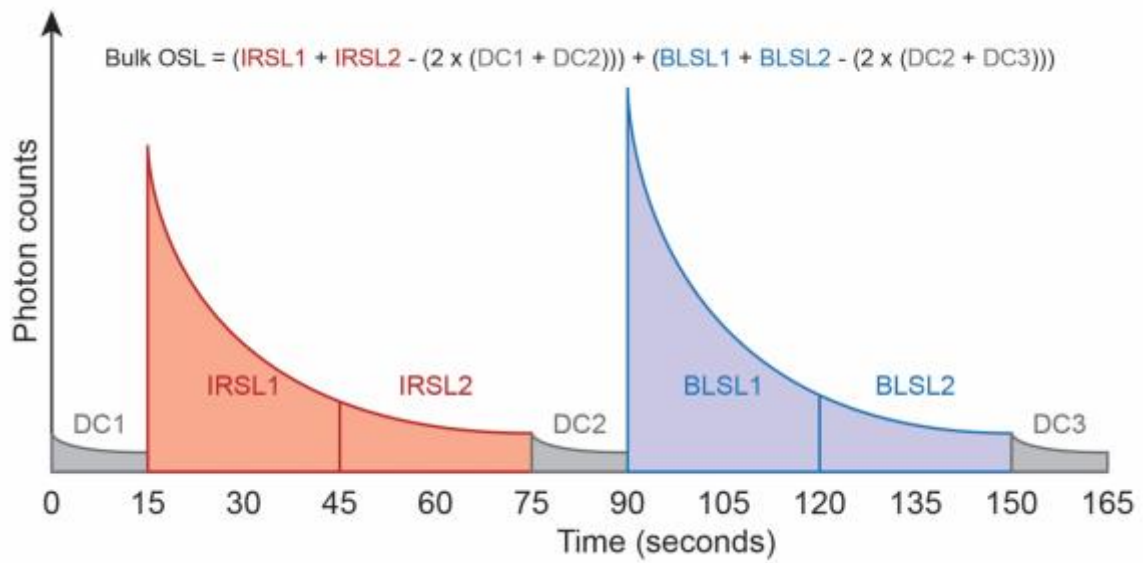


Figure S1. Graphical description of bulk optically stimulated luminescence (bulk OSL) measurements. DC = dark count (luminescence measured in the absence of stimulation); IRSL = infrared stimulated luminescence; BLSL = blue-light LED stimulated luminescence. Equation shows calculation of bulk OSL measurements, which are used in this study.

<i>PSA-1</i>		<i>SM-1</i>		<i>PSA-2</i>		<i>VF-2</i>	
Total OSL		Total OSL		Total OSL		Total OSL	
Depth (cm)	(photon counts) $\times 10^6 \pm \times 10^2$	Depth (cm)	(photon counts) $\times 10^6 \pm \times 10^2$	Depth (cm)	(photon counts) $\times 10^6 \pm \times 10^2$	Depth (cm)	(photon counts) $\times 10^6 \pm \times 10^2$
3	0.58 ± 0.58	3	0.25 ± 0.40	3	0.11 ± 0.49	3	0.51 ± 0.55
6	1.00 ± 0.63	6	0.38 ± 0.43	6	0.17 ± 0.51	6	2.21 ± 0.70
9	1.11 ± 0.64	9	0.44 ± 0.44	9	0.24 ± 0.53	9	3.44 ± 0.76
12	0.90 ± 0.63	12	0.57 ± 0.47	12	0.31 ± 0.55	12	3.56 ± 0.77
15	0.77 ± 0.62	15	0.68 ± 0.48	15	0.39 ± 0.56	15	3.66 ± 0.77
18	1.41 ± 0.68	18	0.80 ± 0.50	18	0.52 ± 0.58	18	2.73 ± 0.73
21	1.12 ± 0.65	21	1.19 ± 0.54	21	0.61 ± 0.59	21	1.82 ± 0.68
24	0.68 ± 0.62	24	1.44 ± 0.56	24	0.73 ± 0.61	24	1.66 ± 0.67
27	0.74 ± 0.62	27	1.87 ± 0.59	27	0.85 ± 0.62	27	1.11 ± 0.63
30	0.92 ± 0.64	30	1.88 ± 0.59	30	1.02 ± 0.64	30	0.86 ± 0.61
33	1.30 ± 0.68	33	2.49 ± 0.63	33	1.17 ± 0.65	33	1.56 ± 0.67
36	1.71 ± 0.72	36	2.88 ± 0.65	36	1.43 ± 0.68	36	0.99 ± 0.63
39	2.23 ± 0.74	39	3.80 ± 0.69	39	1.55 ± 0.69	39	0.98 ± 0.63
42	2.66 ± 0.76	42	3.78 ± 0.69	42	1.65 ± 0.69	42	1.06 ± 0.64
45	2.11 ± 0.73	45	4.44 ± 0.72	45	1.81 ± 0.71	45	1.15 ± 0.65
48	2.04 ± 0.72	48	5.17 ± 0.75	48	2.36 ± 0.74	48	1.25 ± 0.66
51	1.91 ± 0.74	51	4.44 ± 0.72	51	2.08 ± 0.72	51	2.82 ± 0.75
54	2.72 ± 0.78	54	4.86 ± 0.74	54	2.55 ± 0.75	54	1.97 ± 0.71
57	5.43 ± 0.87	57	5.38 ± 0.76	57	2.46 ± 0.75	57	2.12 ± 0.72
60	1.61 ± 0.71	60	4.73 ± 0.74	60	2.25 ± 0.74	60	2.16 ± 0.72
63	1.44 ± 0.69	63	5.92 ± 0.78	63	1.84 ± 0.72	63	2.27 ± 0.73
66	1.90 ± 0.72	66	5.47 ± 0.76	66	1.41 ± 0.69	66	2.93 ± 0.76
69	1.12 ± 0.67	69	7.19 ± 0.81	69	1.16 ± 0.67	69	3.29 ± 0.78
72	0.99 ± 0.66	72	4.21 ± 0.73	72	0.98 ± 0.65	72	3.92 ± 0.81
75	1.02 ± 0.66	75	5.28 ± 0.76	75	1.27 ± 0.68	75	5.79 ± 0.87
78	1.00 ± 0.66	78	4.90 ± 0.75	78	1.61 ± 0.71	78	5.55 ± 0.87
81	1.83 ± 0.72	81	4.46 ± 0.74	81	1.88 ± 0.73	81	6.48 ± 0.89
84	1.54 ± 0.70	84	3.75 ± 0.71	84	2.01 ± 0.73	84	6.42 ± 0.89
87	1.12 ± 0.67	87	3.94 ± 0.73	87	3.13 ± 0.79	87	3.72 ± 0.80
90	0.85 ± 0.64	90	3.02 ± 0.68	90	2.75 ± 0.78	90	5.42 ± 0.86
93	0.69 ± 0.63	93	1.91 ± 0.62			93	5.00 ± 0.85
96	0.37 ± 0.58	96	1.96 ± 0.63			96	4.38 ± 0.94
99	0.25 ± 0.56	99	2.37 ± 0.65			99	5.77 ± 0.88
102	0.09 ± 0.52	102	3.18 ± 0.70			102	6.70 ± 0.91
105	0.08 ± 0.52	107	4.89 ± 0.77				
108	0.08 ± 0.52	112	10.25 ± 0.91				
111	0.08 ± 0.28	117	4.91 ± 0.76				
114	0.12 ± 0.29	122	4.77 ± 0.75				
		127	10.51 ± 0.91				
		132	6.73 ± 0.82				
		137	5.24 ± 0.77				
		142	5.69 ± 0.79				
		147	2.96 ± 0.68				

Table S1. Bulk optically stimulated luminescence (bulk OSL) measurements used in this study

PSA-1			SM-1			PSA-2			VF-1		
SUERC Depth	$^{10}\text{Be}_m$		SUERC Depth	$^{10}\text{Be}_m$		SUERC Depth	$^{10}\text{Be}_m$		SUERC Depth	$^{10}\text{Be}_m$	
BE # ^a	(cm)	(atoms/g) $\times 10^{8b}$	BE # ^a	(cm)	(atoms/g) $\times 10^{8b}$	BE # ^a	(cm)	(atoms/g) $\times 10^{8b}$	BE # ^a	(cm)	(atoms/g) $\times 10^{8b}$
b8029	3	5.81 ± 0.15	b8046	3	8.28 ± 0.16	b8070	3	7.97 ± 0.16	b8048	3	4.29 ± 0.13
b8030	12	7.41 ± 0.17	b8047	15	9.95 ± 0.20	b8072	12	7.82 ± 0.15	b8049	12	3.60 ± 0.09
b8031	21	16.25 ± 0.29	b8056	27	9.76 ± 0.23	b8073	21	7.70 ± 0.16	b8050	21	8.90 ± 0.19
b8033	30	6.94 ± 0.13	b8057	39	10.47 ± 0.17	b8074	30	8.62 ± 0.19	b8053	33	12.82 ± 0.23
b8034	39	7.23 ± 0.14	b8059	51	14.91 ± 0.38	b8075	39	8.55 ± 0.14	b8054	45	14.52 ± 0.36
b8035	48	7.15 ± 0.13	b8060	63	18.59 ± 0.44	b8076	48	6.95 ± 0.13	b8055	54	19.32 ± 0.49
b8036	57	6.70 ± 0.13	b8088	63 ^c	18.85 ± 0.34	b8079	57	9.73 ± 0.20	b8082	63	19.72 ± 0.35
b8037	66	7.39 ± 0.12		63 ^d	18.72 ± 0.39	b8080	66	16.46 ± 0.34	b8083	72	17.66 ± 0.30
b8040	75	8.49 ± 0.18	b8061	75	10.95 ± 0.22	b8081	75	16.85 ± 0.30	b8087	81	15.90 ± 0.33
b8069	84	7.66 ± 0.14	b8066	87	13.85 ± 0.25						
b8043	93	8.78 ± 0.19	b8067	99	20.86 ± 0.39						
b8044	102	14.43 ± 0.28									

^a Original Scottish Universities Environmental Research Centre (SUERC) AMS data report identifying number.

^b Errors presented are 1 σ blank-corrected analytical AMS uncertainties.

^c Replicate measurement of $^{10}\text{Be}_m$

^d The average of $^{10}\text{Be}_m$ data from 63 cm and the replicate from 63 cm. Only the average value is used for analyses in this study.

Table S2. Meteoric ^{10}Be ($^{10}\text{Be}_m$) data used in this study